Contract No.:

This manuscript has been authored by Battelle Savannah River Alliance (BSRA), LLC under Contract No. 89303321CEM000080 with the U.S. Department of Energy (DOE) Office of Environmental Management (EM).

Raman and Infrared Spectra of Plutonium (IV) Oxalate and Its Thermal Degradation Products

Jonathan H. Christian[a,b], Bryan J. Foley[a], Elodia Ciprian[b], Don D. Dick[c], Meena Said[b,d], Jason Darvin[c], Amy Hixon[b*], Eliel Villa-Aleman[c*]

[a] Chemical Processing Section, Savannah River National Laboratory, Aiken, SC 29808 USA
[b] Department of Civil & Environmental Engineering & Earth Sciences, University of Notre Dame, Notre Dame, IN, 46556, USA
[c] Nuclear Nonproliferation Division, Savannah River National Laboratory, Aiken, SC 29808 USA
[d] Nuclear & Chemical Sciences Division, Lawrence Livermore National Laboratory, Livermore, CA, 94550 USA

*Corresponding Authors:
Eliel.Villa-Aleman@srnl.doe.gov
Amy.Hixon.2@nd.edu

Abstract
For over 80 years, plutonium dioxide has been routinely produced via thermal decomposition of hydrated plutonium(IV) oxalate. Despite the longstanding utility of this process, the chemical structures of starting materials and intermediates produced during this thermal conversion remain ill-defined. To help resolve this uncertainty, we measured high-resolution Raman and infrared spectra of $Pu(C_2O_4)_2•6H_2O$ that was heated to 25, 100, 220, 250, 350, and 450 °C in air. Our measurements show that $Pu(C_2O_4)_2•6H_2O$ has a rich vibrational spectrum with at least 15 Raman band between 180 cm^{-1} and 1900 cm^{-1} and 9 infrared bands between 800 cm^{-1} and 4000 cm^{-1}. As $Pu(C_2O_4)_2•6H_2O$ is heated, water is liberated, and the oxalate ligand decomposes to produce plutonium oxycarbide species. When heated to 350 °C or higher, vibrational spectra are consistent with PuO_2 with some residual carbon-containing species. Full vibrational spectra, powder X-ray diffraction, and scanning electron microscopy measurements of $Pu(C_2O_4)_2•6H_2O$ and its thermal degradation products are presented herein along with approximate assignments for observed spectral bands. These data can be used to validate and potentially improve existing computational models that describe the chemical structure of compounds produced during thermal degradation of plutonium (IV) oxalate. Given the utility of plutonium (IV) oxalate in synthesizing plutonium dioxide, these results are expected to provide value in the fields of nuclear fuel processing, nuclear nonproliferation, and nuclear forensics.

Keywords: plutonium oxalate, plutonium dioxide, thermal degradation, calcination, nonproliferation, nuclear forensics

1. Introduction

Conversion of plutonium(IV) oxalate ($Pu(C_2O_4)_2$) to plutonium dioxide (PuO_2) via high-temperature calcination – a process commonly referred to as the Pu(IV) oxalate method – has been utilized for plutonium processing since the 1940s.[1] Due to its simplicity and dependability, the Pu(IV) oxalate method remains the standard for producing PuO_2 at industrial-scale nuclear fuel reprocessing facilities.[2] Despite the enduring utility of this method, and the numerous reports written about it, uncertainty abounds regarding the chemicophysical changes that occur during thermal decomposition of $Pu(C_2O_4)_2$. In fact, there are at least 8 different reports in the literature whose titles contain both the terms “thermal decomposition” and “plutonium (IV) oxalate”. Although many of these reports expound similar results, subtle differences are reported in chemical speciation and degradation temperatures.[3-10] Thermogravimetric analysis (TGA) has been the primary method to assess degradation in the majority of historical reports; however, a 2007 report monitored the degradation using a combination of TGA, powder X-ray diffraction (pXRD), infrared (IR) spectroscopy, and UV-vis spectroscopy, thus providing the most detailed analysis of $Pu(C_2O_4)_2$ decomposition to date.[11] These reports and more are well summarized in a 2015 review.[12]

While these reports vary in their details, several consistencies have been established. First, Pu(IV) oxalate hexahydrate ($Pu(C_2O_4)_2•6H_2O$) is the chemical species formed when oxalic acid is mixed with an acidic Pu(IV) nitrate solution – a result clearly established by XRD analysis.[7, 13] Second, heating $Pu(C_2O_4)_2•6H_2O$ causes dehydration to the dihydrate ($Pu(C_2O_4)_2•2H_2O$) and eventually anhydrous ($Pu(C_2O_4)_2$) phases.[7, 11] Third, isolation of anhydrous and monohydrate Pu(IV) oxalate is difficult due to their hygroscopic nature.[11] Fourth, the oxalate ligand decomposes with sufficient heating, eventually leading to the formation of PuO_2.[14]

Exact chemical structures of species formed as the oxalate ligand decomposes is an area of uncertainty that still surrounds $Pu(C_2O_4)_2$ degradation. The most informative descriptions on this

topic have derived structural details from geometrically-optimized computational models that – with the exception of $Pu(C_2O_4)_2•6H_2O$ and $Pu(C_2O_4)_2•2H_2O$, which have published pXRD patterns – have not been experimentally verified.[7, 10, 13, 15, 16] In fact, a 2021 density functional theory (DFT) study of $Pu(C_2O_4)_2$ decomposition clearly states that the precise structural modifications occurring during thermal decomposition of $Pu(C_2O_4)_2$ have not been experimentally characterized, but the DFT-derived intermediate structures should be identifiable using spectroscopic techniques.[10]

Despite over 80 years of research involving the Pu(IV) oxalate method, no Raman spectra of $Pu(C_2O_4)_2•6H_2O$ or its degradation products have been reported; the lone exception is the Raman spectrum of the terminal degradation product, PuO_2.[17-25]. Although IR data has been published on this topic, the precise energy of all spectral bands from unsaturated spectra using unadulterated sample preparation techniques has not been published.[8, 9, 11] Recognizing the lack of experimentally-measured structural information for compounds formed during Pu(IV) oxalate calcination, we executed high-resolution Raman and IR spectroscopy measurements on $Pu(C_2O_4)_2•6H_2O$ and its degradation products that form up to 450 °C in air. Our experimental setup allowed for collection of high-resolution infrared data under an inert atmosphere using Diffuse Reflectance Infrared Fourier Transform Spectroscopy (DRIFTS) for the Pu-bearing compounds in a double-walled cell. Although the infrared transmission of our double-walled cell is limited by the BaF_2 windows down to 800 cm^{-1} in contrast to samples analyzed using KBr pellets (400 cm^{-1}) and other resins, our DRIFTS approach of the neat material eliminated band contributions from nujol, epoxy resins, or other protective coatings in the analysis of specimens. Our double-walled cell also eliminated the possible interaction of KBr with the oxalate compound and ambient water and prevented potential band saturation due to material concentration. Further, the cells simplified the methodology for analysis with other spectroscopic techniques and allowed for long term storage of the material.

The same materials were also analyzed with Raman spectroscopy to obtain a complete set of bands. The vibrational spectra presented herein provide details of fundamental importance for these crucial nuclear fuel cycle compounds and can be used in future studies to verify the accuracy of theoretically-derived chemical structures. Considering the ubiquity of the Pu(IV) oxalate method in the nuclear fuel cycle, we believe the publication of these vibrational spectra is long overdue.

2. Experimental Methods

2.1 Plutonium (IV) oxalate hexahydrate preparation

All plutonium syntheses were performed inside negative pressure radiological gloveboxes that permit the safe handling of weapons-grade plutonium (> 93 % ^{239}Pu).

In a 20 mL scintillation vial, $Pu(NO_3)_4$ (2.1 mL; 0.1 M in 3 M HNO_3; 0.21 mmol) was added dropwise over five minutes to a stirring solution of oxalic acid dihydrate at 25 °C (4 mL; 0.12 M in water; 0.48 mmol, 2.3 eq.). This solution was stirred for two hours at 25 °C during which time tan/dark white solids formed, as expected for $Pu(C_2O_4)_2•6(H_2O)$. The suspension was gravity filtered through a filtration apparatus and dried under a positive pressure of argon for 2 hours. Removal of the filter membrane and collection of the tan solid yielded the product as a granular brown solid (See Fig. S1). Yield: 96 mg (87%). The composition of this filtered solid was verified by pXRD (*vide infra)*

2.2 Thermal Degradation

Freshly prepared $Pu(C_2O_4)_2•6(H_2O)$ solid was divided into six glass vials; five of these were placed into a muffle furnace (Thermo Fisher FB1315M) to undergo heating within a negative pressure, air atmosphere radiological glovebox. A heating program was then initiated on the furnace. When establishing a temperature, the furnace set point was set ca. 20 °C below the desired temperature to prevent the temperature of the furnace from exceeding the set point. After the temperature had stabilized, the set point of the furnace was moved to the desired temperature and held for one hour. After one hour, the oven was opened, and a vial was removed. The furnace was then raised to the next temperature. This process was performed at 100, 220, 250, 350, and 450 °C. The removed samples were weighed and transferred into sealed glass vials for storage.

2.3 Spectroscopy Sample Preparation

Solid samples were spotted onto a piece of carbon tape within a patent-pending containment cell. The cell was sealed under an argon environment. All characterization measurements were acquired within one week of sample production to limit the degree of lattice damage due to alpha-radiolysis or moisture uptake.

2.4 Raman Spectroscopy

Raman spectra were acquired on a LabRAM HR800 UV (Horiba Jobin-Yvon) equipped with a iDus CCD (Andor DU416A-LDC-DD) detector with a 2000 × 256 pixel array and 15-µm pixel resolution. Most experiments were conducted by binning the spectral array with a factor of two. The Andor detector was cooled to -92 °C with the help of a water chiller. Labspec 5.78 software was used to control the spectrometer and detector. The software was also used to conduct data manipulations. The excitation laser wavelength (λ) was 514 nm. An 1800 g/mm grating was used in the visible spectral range. Ultra-steep long pass edge filters acquired from Semrock Inc. were used to interrogate the vibrational spectra as close as 50 cm^{-1} to the laser excitation line. Acquisition of all Raman spectra presented herein were conducted at 250 µW to avoid heating the sample, and possibly inducing material decomposition with eventual calcination to form plutonium dioxide. Laser intensity at the sample was controlled with a combination of a half-wave plate and polarizer filters and the microscope objective selection (primarily 50x). Laser power, microscope objective, pixel binning, grating and wavelength spectral region (fluorescence background) contributed to the integration time used during the acquisition of the Raman spectra. The integration time varied from a few seconds to several hours to obtain a high signal to noise ratio. For each integration time, at least two spectra were co-added to remove the contribution of cosmic rays to the spectra.

2.5 Infrared Spectroscopy

Diffuse reflectance infrared spectroscopy was performed with a Nicolet 6700 Fourier transform infrared spectrometer and a microscope. Measurements were recorded with a liquid nitrogen cooled mercury cadmium telluride (MCT) detector. Spectra were recorded in the 800 cm^{-1} and 4000 cm^{-1} spectral window with a 4 cm^{-1} resolution. BaF_2 windows in the double-walled cell limited the transmission in the infrared as low as 800 cm^{-1}. The noise in the data increased significantly in the 900 cm^{-1} to 800 cm^{-1} spectral region. A total of 2024 spectra were averaged during

data acquisition. Spectra were processed with the Kubelka-Munk function in the Omnic software. Two measurements were made on each sample to ensure reproducibility.

2.6 Powder X-ray Diffraction

Due to the radiological hazards associated with plutonium, a single crystal X-ray diffractometer (SC-XRD) was used to acquire powder X-ray diffraction (pXRD) data. This technique can lead to slightly broader diffraction lines compared to standard pXRD measurements. The single crystal instrument provides pXRD patterns using minimal (< 1 mg) sample that is mounted on the end of a glass fiber using epoxy. A Bruker Quazar SC-XRD with monochromated Mo-Kα radiation was used to obtain diffractograms for **Pu-25**, **Pu-100**, **Pu-220**, and **Pu-250**, whereas a Rigaku XtlaLab Synergy-S SC-XRD with monochromated Cu-Kα radiation was used to obtain diffractograms for **Pu-350** and **Pu-450**. XRD analysis of the epoxy used to mount the samples was run separately. The resulting broad, amorphous hump between 4 and 25 2θ was baseline-subtracted using OriginPro graphing software. Lanthanum hexaboride, LaB_6 (Alfa Aesar, 99.5 % purity), was used as an external standard to correct for 2θ displacement and all patterns were converted to Cu-Kα 2θ values in order to allow for direct comparison. A qualitative analysis of diffraction patterns was performed using search-match identification of the experimental XRD pattern to the International Centre for Diffraction Data (ICDD) database of crystal and powder X-ray diffraction pattern using the peak intensity and peak position.[26]

2.7 Scanning Electron Microscopy

Sample morphology was monitored using scanning electron microscopy (SEM). Images of thermally degraded plutonium (IV) oxalate samples were taken with a JEOL JCM-6000 Plus Benchtop SEM with an accelerating voltage of 15 kV. The morphology of each sample was examined through secondary electron mode (SE). All samples were prepared inside a glovebox, and powders were deposited on carbon tape adhered to an aluminum stub. Images were taken with magnifications between 1000x and 10000x.

Quantitative analysis of the morphology of $Pu(C_2O_4)_2•6(H_2O)$ and its thermal degradation products was not possible due to particle complexity. Instead, a lexicon of descriptive terms was used to qualitatively describe differences in particle morphology at 5000x magnification.[27] These lexicon descriptors are emphasized in italics below. Careful consideration was taken to choose SEM images that were representative of each sample morphology.

3. Results

The thermal decomposition of $Pu(C_2O_4)_2•6(H_2O)$ to PuO_2 was characterized with vibrational spectroscopy (Raman and infrared), powder X-ray diffraction (pXRD), and scanning electron microscopy (SEM). Hereafter, all analyzed samples are labeled according to the maximum temperature (in Celsius) at which they were heated. Thus, the $Pu(C_2O_4)_2•6(H_2O)$ starting material, which was not heated in a furnace, is labeled **Pu-25**; samples heated to 100, 220, 250, 350, and 450 °C are labeled **Pu-100**, **Pu-220**, **Pu-250, Pu-350,** and **Pu-450**, respectively. The selected temperatures were derived from previously-reported thermogravimetric data that indicates significant mass changes occur near these temperatures.[11]

As shown in Fig. 1 and Fig. S2, pXRD measurements of the brown solids of plutonium (IV) oxalate isolated at room temperature (**Pu-25**) were consistent with $Pu(C_2O_4)_2•6(H_2O)$ (Powder Diffraction File (PDF) 00-014-0798).[28] Upon heating, $Pu(C_2O_4)_2•6(H_2O)$ exhibited a visible color change, as shown in Fig. S1.

Raman and IR band positions for all measured samples are provided in Table 1. Band assignments were determined by comparison with vibrational spectra of related compounds.[11, 29-31] Acquisition and tabulation of these spectral bands are the most crucial aspect of our study, as these data can be used to assess the accuracy of proposed chemical structures associated with the Pu(IV) oxalate method. While DFT-derived chemical structures have been published for both $Pu(C_2O_4)_2•6(H_2O)$ and $Pu(C_2O_4)_2•2(H_2O)$, at the time of publication, these structures are not sufficient for calculating phonons. Thus, we are unable at this time to provide a quantitative comparison between our experimental spectra and the theoretical vibrational modes corresponding to the proposed structures of the Pu(IV) oxalate hydrates.[10]

3.1 Pu-25

The Raman spectrum of $Pu(C_2O_4)_2•6(H_2O)$ was found to contain 15 bands between 180 cm^{-1} and 1900 cm^{-1} (Fig. 2). The most intense bands in the spectrum were located at 1472, 912, and 504 cm^{-1}. As shown in Table 1, most of these bands can be assigned to chemical moieties that are consistent with the chemical formula, $Pu(C_2O_4)_2•6(H_2O)$. This result, in combination with our pXRD measurements, contributes to our confidence that **Pu-25** is indeed $Pu(C_2O_4)_2•6(H_2O)$; however, it cannot be ruled out that there may be some minor variability in the chemical composition of this bulk material

The IR spectrum of **Pu-25** (Fig. 3) contained 9 bands between 800 cm^{-1} and 2400 cm^{-1} and an intense broad band at ~2700 – 3800 cm^{-1}. The broad band can be described as an agglomerate of bands resulting from symmetric and asymmetric stretch vibrations of hydrogen bonded OH groups due to the abundance of water in the hydrated oxalate structure. Like the Raman spectrum, assigned bands in the IR spectrum are consistent with chemical moieties corresponding to the chemical formula, $Pu(C_2O_4)_2•6(H_2O)$; however, the presence of minor variability in the chemical composition in this bulk material cannot be entirely ruled out. The IR spectrum was quite similar to a previously published spectrum by Vigier et al.[11], albeit with slightly higher spectral resolution as a result of our ability to analyze the neat sample and avoid nujol or other sample coatings. Also, our spectrum was not saturated, which helped provide clear band definition and structure.[11] Typical oxalate species show a band at ~1625 cm^{-1} indicating an interaction of the carbonyl group with bonding.[31] In contrast to most published oxalate work, the band of **Pu-25** at 1728 cm^{-1} is indicative of a free carbonyl stretch. Chemical environment and proximity to other chemical groups can affect bonding via hydrogen bonding or interactions with the Pu atom. The high frequency carbonyl band stretch mode indicates weak interactions with Pu or with water molecules.

As shown in Fig 4, SEM measurements of **Pu-25** revealed *complex monodisperse particles* of *mixed* morphology due to *cubic*, *irregular* crystals and the presence of non-crystalline material. Particle faces appeared to be *subhedral* with *sub angular* edges and *low sphericity*. The overall surface of the particles was *somewhat smooth* with surface *fractures* and *eroded* edges. These observations are consistent with the morphology of plutonium oxalate crystal clusters described by Crowder et al.[32]

3.2 Pu-100

Raman bands for samples heated to 100 °C (**Pu-100)** were nearly identical to **Pu-25** with only slight differences observed in the intensity and full width at half maximum (FWHM) of some bands between ~1550 – 1900 cm^{-1} (Fig. 2). As seen in the IR spectrum of **Pu-100** (Fig. 3), there was a dramatic reduction in the FWHM and intensity of the water bands between ~2400 – 3800 cm^{-1}, thus indicating that water is liberated as the hexahydrate compound is heated. The reduction in FWHM and intensity for the water bands provides a clear distinction between the hexahydrate and the dihydrate oxalate structures.

As shown in Fig. 1 and Fig. S3, pXRD measurements of **Pu-100** were consistent with $Pu(C_2O_4)_2•2(H_2O)$ (PDF 00-018-0982).[33] This result is consistent with the IR showing reduced water content relative to **Pu-25**.

SEM measurements after thermal degradation at 100 °C revealed particles that appeared to have an *individual mixed* morphology (Fig 5a). A majority of the particles had a cubic shape with *subhedral* faces, *sub angular* edges, and *low sphericity*. The overall surface of particles was *rough* with the appearance of surface *layers*, *eroded* edges, and surface *pits*.

3.3 Pu-220 and Pu-250

The Raman spectra of **Pu-220** and **Pu-250** (Fig. 2) were similar to each other but significantly different from the **Pu-25** and **Pu-100** spectra. Specifically, there was a reduction in the intensity and a slight shift in the energy of most bands for **Pu-220 and Pu-250** relative to the lower temperature samples. The most dramatic reductions in band intensity were seen at 504, 912, and 1472 cm^{-1}, which correspond to the C-O, C-C, and delta ring deformation or Pu-O mode within the oxalate, respectively. Reduction in the intensity of these bands is consistent with thermal degradation of the oxalate ligand.[29, 31] A significant number of weak bands were also observed in the spectrum.

In addition to bands associated with oxalate decreasing in intensity with increased temperature, there was a concomitant increase in the Raman band at 1088 cm^{-1}. This band is assigned to a carbonate vibrational mode; therefore, an increase in the intensity indicates carbonate species are progressively replacing the oxalate species at temperatures near 220 °C. This is consistent with the thermogravimetric analysis (TGA) data published by Vigier et al., which showed formation of $Pu(C_2O_4)(CO_3)_{1/2}$, $Pu(C_2O_4)_{1/2}(CO_3)$, and $PuOCO_3$ at temperatures above 210 °C.[11] The carbonate band at 1088 cm^{-1} was observed to lead to the band at 428 cm^{-1} which we assign to $PuOCO_3$. The carbonate band growth observed in the Raman spectrum is consistent with the growth of the CO_2 band in the infrared spectrum at 2343 cm^{-1}.

A change to the spectral baseline occurred between ~1150 cm^{-1} and 1600 cm^{-1} for the 220 and 250 °C samples. This change is tentatively assigned as carbonaceous soot formed during oxalate degradation. Carbonaceous soot typically has large, broad Raman bands at ~1350 cm^{-1} and ~1560 cm^{-1}.[34] A similar broad background was observed in the infrared spectra in the 1100 cm^{-1} to 1800 cm^{-1} spectral region. Given the low amount of heat applied to the system (resulting in incomplete oxalate "burn off") it is reasonable to observe amorphous carbon in the sample as high as 350 °C. The presence of the CO_2 band in the infrared spectra of **Pu-220**, **Pu-250**, and **Pu-350** is also consistent with significant residual carbon in the system.

Pu-220 and **Pu-250** produced a clear and much more intense Raman band at 1382 cm^{-1} that can be ascribed to a symmetric vibration of CO_2. A major difference between the Raman spectra of **Pu-250** and all lower temperature spectra was the shift to higher wavenumbers for the band at ~408

cm^{-1}. For the 250 °C sample, this band shifted to ~428 cm^{-1}, which is likely due to formation of plutonium oxycarbides and is consistent with previous identification of $PuOCO_3$ above 235 °C.[11]

A surprising feature in the **Pu-220** and **Pu-250** Raman spectra was the emergence of a low intensity band near 580 cm^{-1} and a small, broad band near 480 cm^{-1}. Lattice defects from self-radiolysis in PuO_2 produce a similar Raman band near 580 cm^{-1} and the intense T_{2g} band of PuO_2 occurs near 480 cm^{-1}.[17, 18] These results suggest that small amounts of PuO_2 form from Pu(IV) oxalate at temperatures as low as 220 – 250 °C. The T_{2g} band of most PuO_2 (and CeO_2) particles is sharp and symmetric; however, in nanoparticulates, the T_{2g} band broadens and becomes asymmetric.[35] Given that the T_{2g} band we observed at 480 cm^{-1} was broad and asymmetric, it is likely that nanoparticles of PuO_2 were formed. Observation of this result was aided by the ultra-sensitivity of Raman spectroscopy to the T_{2g} band of PuO_2 and the observation of the electronic band at 2640 cm^{-1}. We are unaware of any previous evidence showing PuO_2 formation at such low temperatures.

Infrared spectra of **Pu-220** and **Pu-250 (**Fig. 3) showed reduced water content relative to all lower temperature samples. Another noteworthy feature of the 220 and 250 °C spectra was the significant increase in intensity of the band at 2344 cm^{-1}, which is ascribed to CO_2. Clearly, both Raman and IR spectra show that thermal degradation of the oxalate ligand produces CO_2. Since vibrational spectra were measured a few days after the solid samples had been heated, this CO_2 remains trapped in the solid lattice as adsorbed gas, although elucidation of this trapping mechanism was beyond the scope of our study. Similar observations of CO_2 and possible mechanisms involving CO_2 gas formation during Pu oxalate degradation is described in numerous reports, and is well summarized in a review by Orr et al. [12]

As a free gas, CO_2 produces bands that are significantly broader due to the presence of the rotational envelopes described by the energy levels of the P and R branches. Typical locations of the P and R branch maxima are 2361 cm^{-1} and 2331 cm^{-1}, respectively. In contrast to a free gas, rotation of CO_2 is hindered when it is trapped in a solid, and only one sharp band at 2344 cm^{-1} is observable in the spectrum. This sharp band is a signature of CO_2 that is trapped in the solid and is indicative of carbon (from oxalate) oxidation at elevated temperature. The mechanism by which the CO_2 remains trapped in the solid is unclear at this time.

The infrared spectral region encompassing 1745 – 1200 cm^{-1} describes the internal and external oxalate vibrational modes. The **Pu-25** infrared spectrum is dominated by four bands in this region; 1728, 1606, 1471, 1355, and 1314 cm^{-1}. Most oxalate-bearing compounds are characterized by a strong band at ~1465 cm^{-1} and a weaker satellite band at ~1430 cm^{-1}; both corresponding to the C-O vibrational modes. The **Pu-25** oxalate infrared spectrum shows a strong band at 1728 cm^{-1} and a satellite band 1606 cm^{-1}. The band at 1728 cm^{-1} and most likely the 1606 cm^{-1} band correspond to two different carbonyl groups where one carbonyl group is significantly independent and the other elongated carbonyl is interacting with its neighbors (most likely through hydrogen bonding). A carbonyl stretch of high frequency has significant implications in the bonding of the oxalate and suggest that hydrogen bonding is nonexistent with the carbonyl oxygen since any bonding with the carbonyl oxygen should lower the frequency of the stretch. It is possible that the band at 1606 cm^{-1} corresponds to a portion of the carbonyl groups involved in interactions with surrounding waters. **Pu-100** shows the disappearance of the 1606 cm^{-1} band and a sharpening of the carbonyl band previously located at 1728 cm^{-1} with a shift to higher frequency, 1745 cm^{-1}. The higher frequency stretch of the carbonyl group is indicative of weak interactions with its neighbors at most. The sharp band is also indicative of the oxalate groups having similar distances with the neighbors. In Pu (IV) oxalate, there are four carbonyl groups and one single strong band suggesting similar geometry of the oxalate

groups with their neighbors. The infrared spectra of **Pu-220** and **Pu-250** shows a splitting of the intense band of the carbonyl group into two bands located at 1726 cm^{-1} and 1711 cm^{-1} suggesting different interactions. Concurrent to the carbonyl group split, the bands located at 1600, 1470, 1350, and 1313 cm^{-1} begin to blur into a quasi-continuum absorption. At **Pu-250**, only the carbonyl group and at band at 1348 cm^{-1} dominate the spectrum. The observed wavenumber shifts may correspond to changes from non-bridging to bridging moieties due to thermal degradation taking place. Most likely, the oxygen in the carbonyl is beginning to interact with the Pu atoms in a transition to $PuOCO_3$ and PuO_2.

X-ray diffraction patterns of **Pu-220** and **Pu-250** (Fig. 1) contain several broad features consistent with a chemical structure that is more amorphous than crystalline. As such, these patterns could not be reasonably matched to any diffraction patterns in the ICDD database and suggest that heating $Pu(C_2O_4)_2•2(H_2O)$ up to 220 °C leads to a loss in bulk crystallinity. A similar loss in crystallinity was observed when Desfougeres et al.[30] heated $U(C_2O_4)_2•6(H_2O)$ and measured pXRD of the resultant solid product.

Importantly, over the course of our experiments, several samples heated to 200 °C show extreme sensitivity to temperature variations such that one sample batch could produce a material best described as more amorphous, like **Pu-220,** while a different sample batch could produce a material best described as more crystalline, like **Pu-100**. These inconsistent results suggest there is a threshold temperature near 200 °C where Pu(IV) oxalate undergoes significant structural alterations. Minor and intrinsic variations in furnace temperature/thermal gradients within the furnace are likely why different batches were not consistent with each other. This result is consistent with previously published TGA data by Vigier et al.,[11] which showed that anhydrous Pu(IV) oxalate undergoes significant degradation between 180 – 210 °C. Given the thermal sensitivity near 200 °C, we postulate that plutonium oxalate degradation may occur by catalytic action of evolved gases. CO_2 was clearly observed in our IR and Raman measurements; however, we are less certain about the formation of CO. Numerous reports, some with conflicting conclusions, have described the evolution of CO_2 and CO gases during Pu(IV) oxalate degradation, and CO gas has been observed to catalytically enhance the degradation of ytterbium oxalate.[36]. A complete review of these reports and the chemistry involving CO_2 gas evolution is beyond the scope of our vibrational spectroscopy study; therefore, we direct the reader to an excellent review paper on the topic.[12]

The morphology of **Pu-220** was consistent with **Pu-100** (Figure 5b). Particles appeared to have an *individual bimodal mixed* morphology, including *cubic* and *irregular* shapes, with *subhedral* faces, *sub angular* edges, and *low sphericity*. The overall surface of particles was *rough* with surface *layers*, *eroded* edges, and *fines*. The particle morphology of **Pu-250** (Figure 5c) was consistent with **Pu-100** (i.e., *subhedral* faces with *sub angular* edges and *low sphericity*). However, the overall surface of **Pu-250** could be described as *rough* with *dissolved* surfaces and *eroded* edges. It also displayed *layered* features.

3.4 *Pu-350 and Pu-450*

Raman spectra of **Pu-350** and **Pu-450** (Fig. 2) are clearly consistent with PuO_2, a compound that our group has extensively characterized by Raman spectroscopy in the past.[17, 18, 20] Some residual carbon species from oxalate degradation are also found in the spectra. The Raman spectrum of **Pu-350** exhibited greater intensity of the PuO_2 T_{2g} band and its corresponding defect band region (~580 – 650 cm^{-1}). The defect band observed in **Pu-450** Raman spectrum was significantly weaker than the band in the **Pu-350** , which is consistent with annealing of defects in the crystal lattice .[17]

IR spectra of **Pu-350** and **Pu-450** were similar with the primary difference being reduced FWHM and intensity for most of the features in **Pu-450** relative to **Pu-350**. This observation is a result of the material being more crystalline due to the higher calcination temperature and is consistent with pXRD measurements (*vide infra*). IR spectra of both samples showed bands that we attribute to the presence of Pu oxycarbides. Reduction of the intensity of these bands was observed by calcining to the higher temperature of 450 °C. Importantly, as shown in Table 1, there are clearly a number of residual carbon species present in **Pu-350** and **Pu-450**. The presence of residual carbon is consistent with previous observations by Nissen,[8] which show that as much as 5,000 ppm of carbon can remain in PuO_2 after it is formed from calcination of plutonium oxalate.

As shown in Fig. 1 and Fig. S4, pXRD diffractograms of both **Pu-350** and **Pu-450** were an excellent match to the ICDD patterns for PuO_2 (PDF 00-067-0018).[37] The FWHM of diffraction peaks was lower for **Pu-450** compared to **Pu-350**, thus suggesting the material calcined at a higher temperature is more crystalline. Consistent with the vibrational spectra of these samples, which indicated the presence of some residual carbon species, the pXRD patterns of **Pu-350** and **Pu-450** both contain an amorphous feature centered at ~20 2θ that could not be reasonably matched to any diffraction patterns in the ICDD database. A similar feature was observed in the pXRD patterns of **Pu-220** and **Pu-250**, thus indicating that some amorphous material remains in both **Pu-350** and **Pu-450**.

The particle morphology of **Pu-350** (Figure 5d) was consistent with **Pu-100** (i.e., *subhedral* faces with *sub angular* edges and *low sphericity*), whereas the overall surface was consistent with **Pu-250**. The overall surface of **Pu-350** was *rough* with *dissolved* surfaces and *eroded* edges, *layers,* and *pits*. The surface and particle morphology of **Pu-450** (Figure 5e) was consistent with **Pu-350**. Particles appeared *subhedral* with *sub angular* edges and *low sphericity*. The overall surface of particles was *rough* with the appearance of *layers, eroded edges dissolved surface,* and *pits.* A review of the literature suggests that the morphology of PuO_2 formed through the Pu(IV) oxalate process can differ based on the parameters and conditions chosen during sample preparation. For example, Said and Hixon[38] describe such PuO_2 as crystalline complex particles displaying columnar or equiaxed crystal shape with tabular sub particles that combine to form rosette-like aggregates, whereas others[39, 40] observe tightly packed platelets that form spherical PuO_2 particles. More generally, PuO_2 produced through the oxalate process has been described as rosettes, square prisms, or thin plates.[12]

4. Discussion

Elucidating the structure and reactivity of nuclear materials is a fundamental goal for nuclear fuel processing, nuclear nonproliferation, and nuclear forensics. Vibrational spectroscopy is a useful tool for identifying chemical composition and was utilized herein along with ancillary pXRD and SEM measurements to evaluate $Pu(C_2O_4)_2•6(H_2O)$ and its thermal degradation products. These results paint a vivid picture of the mechanism associated with conversion from $Pu(C_2O_4)_2•6(H_2O)$ to PuO_2 and help elucidate this complex degradation mechanism which has been a subject of uncertainty for at least 80 years.

Specific chemical details involved in $Pu(C_2O_4)_2•6(H_2O)$ degradation are contained within the results section of this report. In general, the degradation of $Pu(C_2O_4)_2•6(H_2O)$ can be summarized as follows:

- Crystalline Pu(IV) oxalate hexahydrate ($Pu(C_2O_4)_2•6H_2O$) is the chemical species formed when oxalic acid is mixed with an acidic Pu(IV) nitrate solution; a result clearly established by all of our analytical measurements.
- $Pu(C_2O_4)_2•6H_2O$ has a rich vibrational spectrum with at least 15 Raman and 9 infrared bands between 180 – 1900 cm^{-1}.
- As $Pu(C_2O_4)_2•6H_2O$ is heated to 100 °C, water is liberated to produce crystalline $Pu(C_2O_4)_2•2H_2O$, which also has a rich vibrational spectrum that is similar to the spectrum of $Pu(C_2O_4)_2•6H_2O$, albeit with a dramatic reduction in the FWHM and intensity of the water bands between ~ 2400 – 3800 cm^{-1}. Reduction in the FWHM and intensity of the water bands allows the dihydrate structure to be clearly differentiated from the hexahydrate structure.
- As $Pu(C_2O_4)_2•2H_2O$ is heated above 100 °C, the oxalate ligand decomposes to produce amorphous plutonium oxycarbide species, CO_2, and ultimately crystalline PuO_2 with some residual carbon-containing species remaining up to 450 °C
- Small amounts of PuO_2 were found at calcination temperatures as low as 220 - 250°C. Observation of this result was aided by the ultra-sensitivity of Raman spectroscopy to the T_{2g} band. We are unaware of any previous evidence showing PuO_2 formation at such low temperatures.

5. Conclusions

High-resolution Raman and IR spectra were measured for $Pu(C_2O_4)_2•6(H_2O)$ and its thermal degradation products that were produced by heating $Pu(C_2O_4)_2•6(H_2O)$ to 100, 220, 250, 350, and 450 °C. Oxalate degradation leading to plutonium oxycarbide(s) formation was observed *en route* to PuO_2 formation. CO_2 was observed in samples heated above 220 °C, which is consistent with previous reports on oxalate degradation.[12] With significant spectral averaging and careful selection of spectrometer settings, all measured samples exhibited rich vibrational spectra that provide a detailed look at the structural and bonding characteristics of the resultant products. In general terms, our spectra certainly do not disagree with previously published DFT structures for hydrated oxalates in that we observed vibrational bands corresponding to oxalate, water, Pu-O, etc.; however, additional DFT calculations are needed to produce the exact phonons from the hydrated oxalate structures in order to compare them with the energies measured by Raman and IR. Hereafter, the detailed vibrational spectra published herein can be used to assess the accuracy of proposed Pu(IV) oxalate structures.[10]

Declaration of Competing Interest

The authors declare that they have no known competing financial interests or personal relationships that could have appeared to influence the work reported in this paper.

Abbreviations

DFT – density functional theory
DRIFTS – Diffuse Reflectance Infrared Fourier Transform Spectroscopy
FWHM – full width at half maximum
IR – infrared
pXRD – powder X-ray diffraction
SEM – scanning electron microscopy

S/N – signal to noise
TGA – thermogravimetric analysis

Acknowledgements
This work was produced by Battelle Savannah River Alliance, LLC under Contract No. 89303321CEM000080 and/or a predecessor contract with the U.S. Department of Energy. Publisher acknowledges the U.S. Government license to provide public access under the DOE Public Access Plan (http://energy.gov/downloads/doe-public-access-plan). This work was sponsored by the DOE National Nuclear Security Administration Office. The authors wish to acknowledge the SRNL Laboratory Directed Research & Development under the project LDRD-2016-00015 for procurement of some spectroscopy equipment and investment in project development.

References

[1] O.J. Wick, Plutonium Handbook: A Guide to the Technology, American Nucear Society, La Grange Park, IL, 1980.
[2] J.P. Patterson, P. Parkes, Recycling uranium and plutonium, Oxford University Press, United Kingdom, 1996.
[3] M.N. Myser, Thermal Decomposition of Plutonium(IV) Oxalate and Hydrofluorination of Plutonium(IV) Oxalate and Oxide, United States: N. p., 1956. Web. doi:10.2172/4181389.
[4] R.E. Kartushova, T.I. Rudenko, V.V. Fomin, Thermal decomposition of tetravalent and trivalent plutonium oxalates, The Soviet Journal of Atomic Energy 5(1) (1958) 831-835.
[5] G.S. Rao, M.S. Subramanian, G.A. Welch, Thermal decomposition of plutonium oxalates, Journal of Inorganic and Nuclear Chemistry 25(10) (1963) 1293-1295.
[6] A. Glasner, Remarks on the thermal decomposition of plutonium (IV) oxalates, Journal of Inorganic and Nuclear Chemistry 26(8) (1964) 1475-1476.
[7] I.L. Jenkins, M.J. Waterman, The thermal decomposition of hydrated plutonium(IV) oxalates, Journal of Inorganic and Nuclear Chemistry 26(1) (1964) 131-137.
[8] D.A. Nissen, The thermal decomposition of Plutonium (IV) oxalate hexahydrate, Journal of thermal analysis 18(1) (1980) 99-109.
[9] A.I. Karelin, N.N. Krot, R.D. Kozlova, O.P. Lobas, V.A. Matukha, Thermal decomposition of Np(IV) and Pu(III, IV) oxalates, Journal of Radioanalytical and Nuclear Chemistry Articles 143(1) (1990) 241-252.
[10] C.J. South, L.E. Roy, Insights into the thermal decomposition of plutonium(IV) oxalate – a DFT study of the intermediate structures, Journal of Nuclear Materials 549 (2021) 152864.
[11] N. Vigier, S. Grandjean, B. Arab-Chapelet, F. Abraham, Reaction mechanisms of the thermal conversion of Pu(IV) oxalate into plutonium oxide, Journal of Alloys and Compounds 444-445 (2007) 594-597.
[12] R.M. Orr, H.E. Sims, R.J. Taylor, A review of plutonium oxalate decomposition reactions and effects of decomposition temperature on the surface area of the plutonium dioxide product, Journal of Nuclear Materials 465 (2015) 756-773.
[13] I.L. Jenkins, Moore, F. H., Waterman, M. J., Chem. and Indus. 35 (1963).
[14] J.M. Cleveland, Section IV: Chemical Processing in Plutonium Handbook: A Guide to the Technology, LaGrange Park, IL, American Nuclear Society, 1980.
[15] K.E. Garrett, A.M. Ritzmann, F.N. Smith, S.H. Kessler, R. Devanathan, N.J. Henson, D.G. Abrecht, First principles investigation of the structural and bonding properties of hydrated actinide

(IV) oxalates, An(C2O4)2·6H2O (An = U, Pu), Computational Materials Science 153 (2018) 146-152.
[16] F. Abraham, B. Arab-Chapelet, M. Rivenet, C. Tamain, S. Grandjean, Actinide oxalates, solid state structures and applications, Coordination Chemistry Reviews 266-267 (2014) 28-68.
[17] E. Villa-Aleman, D.D. Dick, J.H. Christian, B.J. Foley, Laser-induced annealing of aged PuO2, Journal of Raman Spectroscopy 52(8) 1486-1489.
[18] E. Villa-Aleman, N.J. Bridges, T.C. Shehee, A.L. Houk, Raman microspectroscopy of PuO2 particulate aggregates, Journal of Nuclear Materials 515 (2019) 140-149.
[19] E. Villa-Aleman, A.L. Houk, T.C. Shehee, N.J. Bridges, Raman signatures from age-dating PuO2 since last calcination, Journal of Nuclear Materials 551 (2021) 152969.
[20] E. Villa-Aleman, A.L. Houk, N.J. Bridges, T.C. Shehee, Raman spectroscopy: A tool to investigate alpha decay damage in a PuO2 crystal lattice and determining sample age since calcination, Journal of Raman Spectroscopy 50(6) (2019) 899-901.
[21] M.J. Sarsfield, R.J. Taylor, C. Puxley, H.M. Steele, Raman spectroscopy of plutonium dioxide and related materials, Journal of Nuclear Materials 427(1) (2012) 333-342.
[22] C. Jégou, R. Caraballo, S. Peuget, D. Roudil, L. Desgranges, M. Magnin, Raman spectroscopy characterization of actinide oxides (U1−yPuy)O2: Resistance to oxidation by the laser beam and examination of defects, Journal of Nuclear Materials 405(3) (2010) 235-243.
[23] M. Naji, N. Magnani, L.J. Bonales, S. Mastromarino, J.Y. Colle, J. Cobos, D. Manara, Raman spectrum of plutonium dioxide: Vibrational and crystal field modes, Physical Review B 95(10) (2017) 104307.
[24] G.M. Begun, R.G. Haire, W.R. Wilmarth, J.R. Peterson, Raman spectra of some actinide dioxides and of EuF2, Journal of the Less Common Metals 162(1) (1990) 129-133.
[25] D. Manara, M. Naji, S. Mastromarino, J.M. Elorrieta, N. Magnani, L. Martel, J.Y. Colle, The Raman fingerprint of plutonium dioxide: Some example applications for the detection of PuO2 in host matrices, Journal of Nuclear Materials 499 (2018) 268-271.
[26] S. Gates-Rector, T. Blanton, The Powder Diffraction File: a quality materials characterization database, Powder Diffraction 34(4) (2019) 352-360.
[27] A.L. Tamasi, L.J. Cash, C. Eley, R.B. Porter, D.L. Pugmire, A.R. Ross, C.E. Ruggiero, L. Tandon, G.L. Wagner, J.R. Walensky, A.D. Wall, M.P. Wilkerson, A lexicon for consistent description of material images for nuclear forensics, Journal of Radioanalytical and Nuclear Chemistry 307(3) (2016) 1611-1619.
[28] PDF 4 Database, International Centre for Diffraction Data, Newtown Square, PA, 2015, Card No #00-014-0798, PDF 4 Database, International Centre for Diffraction Data, Newtown Square, PA, 2015, Card No #00-014-0798.
[29] K. Nakamoto, Infrared and Raman Spectra of Inorganic and Coordination Compounds - Application in Coordination, Organometallic, and Bioinorganic Chemistry, Wiley, Hoboken, NJ, 2009.
[30] L. Desfougeres, É. Welcomme, M. Ollivier, P.M. Martin, J. Hennuyer, M.O.J.Y. Hunault, R. Podor, N. Clavier, L. Favergeon, Oxidation as an Early Stage in the Multistep Thermal Decomposition of Uranium(IV) Oxalate into U3O8, Inorganic Chemistry 59(12) (2020) 8589-8602.
[31] R.L. Frost, M.L. Weier, Raman spectroscopy of natural oxalates at 298 and 77 K, Journal of Raman Spectroscopy 34(10) (2003) 776-785.
[32] M.L. Crowder, R.A. Pierce, J.H. Scogin, W.E. Daniel, W.D. King, Small-scale Testing of Plutonium(IV) Oxalate Precipitation and Calcination to Plutonium Oxide to Support the MOX Feed Mission (SNRL-STI-2012-00338) (2012) 1-53.

[33] PDF 4 Database, International Centre for Diffraction Data, Newtown Square, PA, 2015, Card No #00-018-0982, PDF 4 Database, International Centre for Diffraction Data, Newtown Square, PA, 2015, Card No #00-018-0982.
[34] A. Sadezky, H. Muckenhuber, H. Grothe, R. Niessner, U. Pöschl, Raman microspectroscopy of soot and related carbonaceous materials: Spectral analysis and structural information, Carbon 43(8) (2005) 1731-1742.
[35] I. Kosacki, T. Suzuki, H.U. Anderson, P. Colomban, Raman scattering and lattice defects in nanocrystalline CeO2 thin films, Solid State Ionics 149(1) (2002) 99-105.
[36] A. Glasner, E. Levy, M. Steinberg, Thermal decomposition of ytterbium oxalate, Journal of Inorganic and Nuclear Chemistry 26(7) (1964) 1143-1149.
[37] PDF 4 Database, International Centre for Diffraction Data, Newtown Square, PA, 2015, Card No #00-067-0018, PDF 4 Database, International Centre for Diffraction Data, Newtown Square, PA, 2015, Card No #00-067-0018.
[38] M. Said, A.E. Hixon, Microscopy and spectroscopy of plutonium dioxide aging under ambient and near-ambient conditions, Journal of Alloys and Compounds 854 (2021) 156277.
[39] P.C. Doto, C.M. Peabody, Production of Ceramic Grade Plutonium Dioxide, (ARH-SA-213, Richland) (1975) 1-16.
[40] D.T. Rankin, G.A. Burney, Particle Size of $^{238}PuO_2$ Obtained by Oxalate Precipitation and Calcination, (DP-MS-74-37, Aiken) (1974) 1-25.

TABLE 1

Band positions for the vibrational spectra of Pu(IV) oxalate ($Pu(C_2O_4)_2$•$6(H_2O)$) produced at room temperature (**Pu-25**) and its degradation products when heated up to 450 ºC (**Pu-450**); band positions in cm^{-1}. Bands of similar wavenumbers are compiled in the same row. When practical, band assignments are listed and are based on comparison with related compounds; bands that could not be unambiguously assigned are not labeled.[11, 29, 30]

Pu-25		**Pu-100**		**Pu-220**		**Pu-250**		**Pu-350**		**Pu-450**		**Approximate vibrational mode assignments**
IR	*Raman*	*IR*	*Raman*	*IR*	*Raman*	*IR*	*Raman*	*IR*	*Raman*	*IR*	*Raman*	
	187		187									Pu-O and lattice
	241		241		241		241					Pu-O and lattice
	399		409		409		428					Pu-O and lattice
					481		481		474		478	T_{2g} of PuO_2
	504		504									δ(OCO)
					581		581		581		581	Defect band of PuO_2
	754		754		754		754					
										802		
								820		827		
								833		847		
876	858		863		846		833	841				
										863		
										879		
												ν(C-C) +
1052	912	976	912	900	916	960	916	935		935		ν(CO) + δ(OCO)
	1070		1063									
										1049		
1120				1037		1161		1075		1131		
				828	1088		1088					ν(CO_3)
									1163		1163	2LO2 of PuO_2
1314	1319	1311		1313	1282		1278			1256		ν(CO) + δ(OCO)
1355		1350		1350	1333	1348	1333					ν(CO) + ν(C-C)
	1388		1388		1382		1382	1386		1362		ν(CO)
	1410		1410									
1471	1472	1480	1472	1474	1478		1480					ν(CO)
								1574		1579		
1606	1620	1590	1611	1621	1606		1608					ν(RCO_2) + ν(RCO)
1728	1715	1745	1715	1711		1702		1742				ν(C=O)
	1818									1880		
1920		1906		1906		1921		1925				
								2156				
								2276				
		2343		2343		2344		2340				ν(CO_2)
Multiple broad bands between 2400 – 3800												ν(OH) + ν(C-H)$_{contamination}$

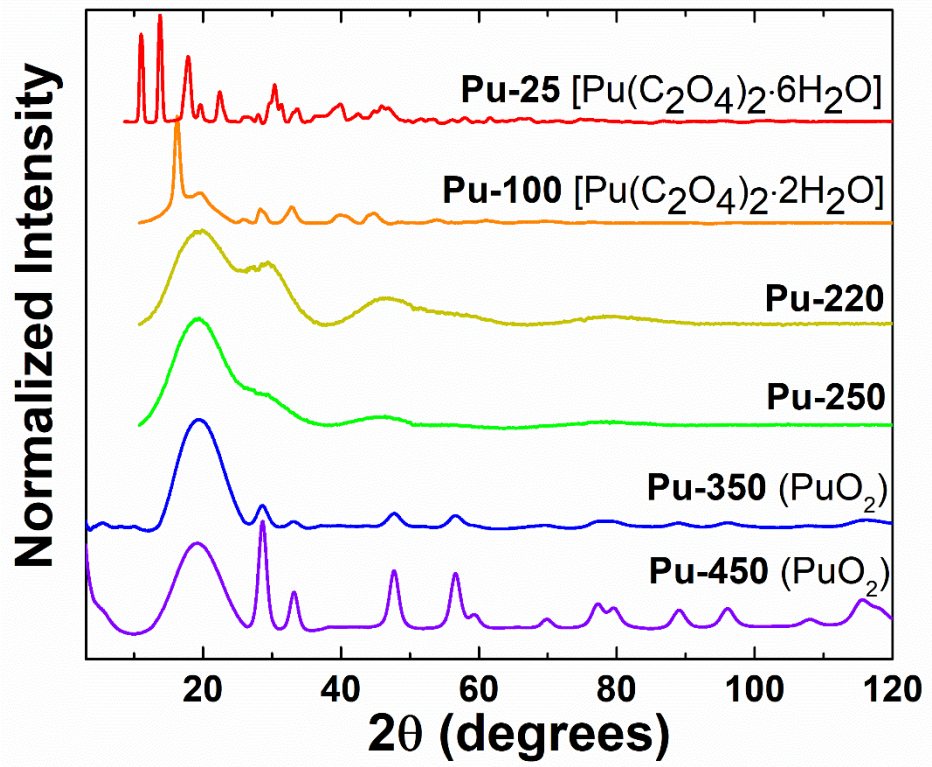

Fig. 1. pXRD patterns of $Pu(C_2O_4)_2$•$6(H_2O)$ produced at room temperature (**Pu-25**) and its degradation products as it is heated to 450 °C (**Pu-450**).

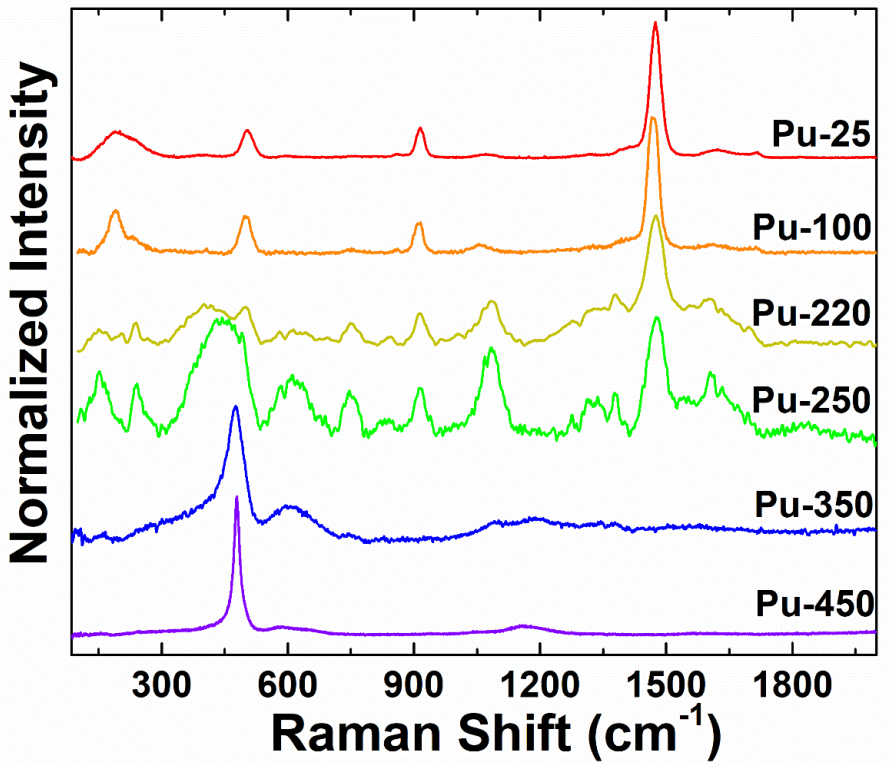

Fig. 2. Raman spectra of $Pu(C_2O_4)_2$•$6(H_2O)$ produced at room temperature (**Pu-25**) and its degradation products as it is heated to 450 °C (**Pu-450**).

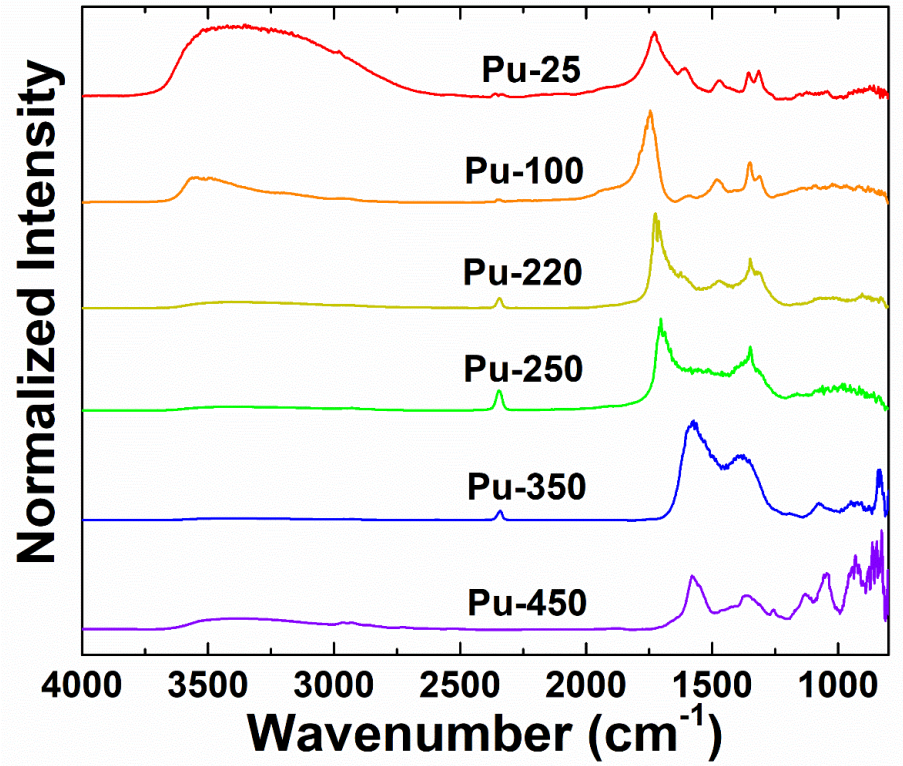

Fig. 3. IR spectra of $Pu(C_2O_4)_2 \cdot 6(H_2O)$ (**Pu-25**) and its degradation products as it is heated to 450 ºC (**Pu-450**).

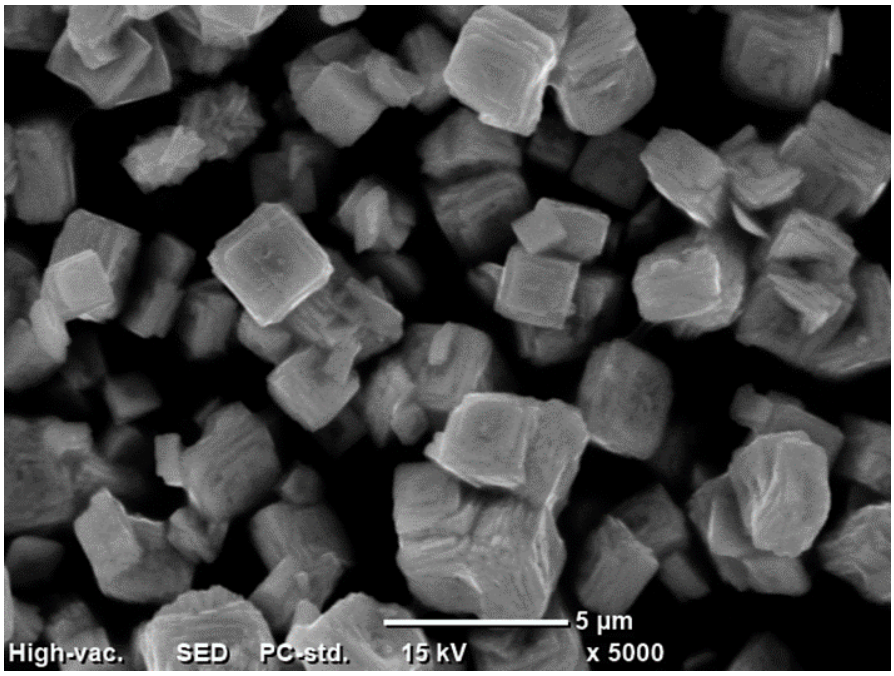

Fig. 4. Scanning electron micrograph of $Pu(C_2O_4)_2 \cdot 6H_2O$ (**Pu-25**) under 5000x magnification.

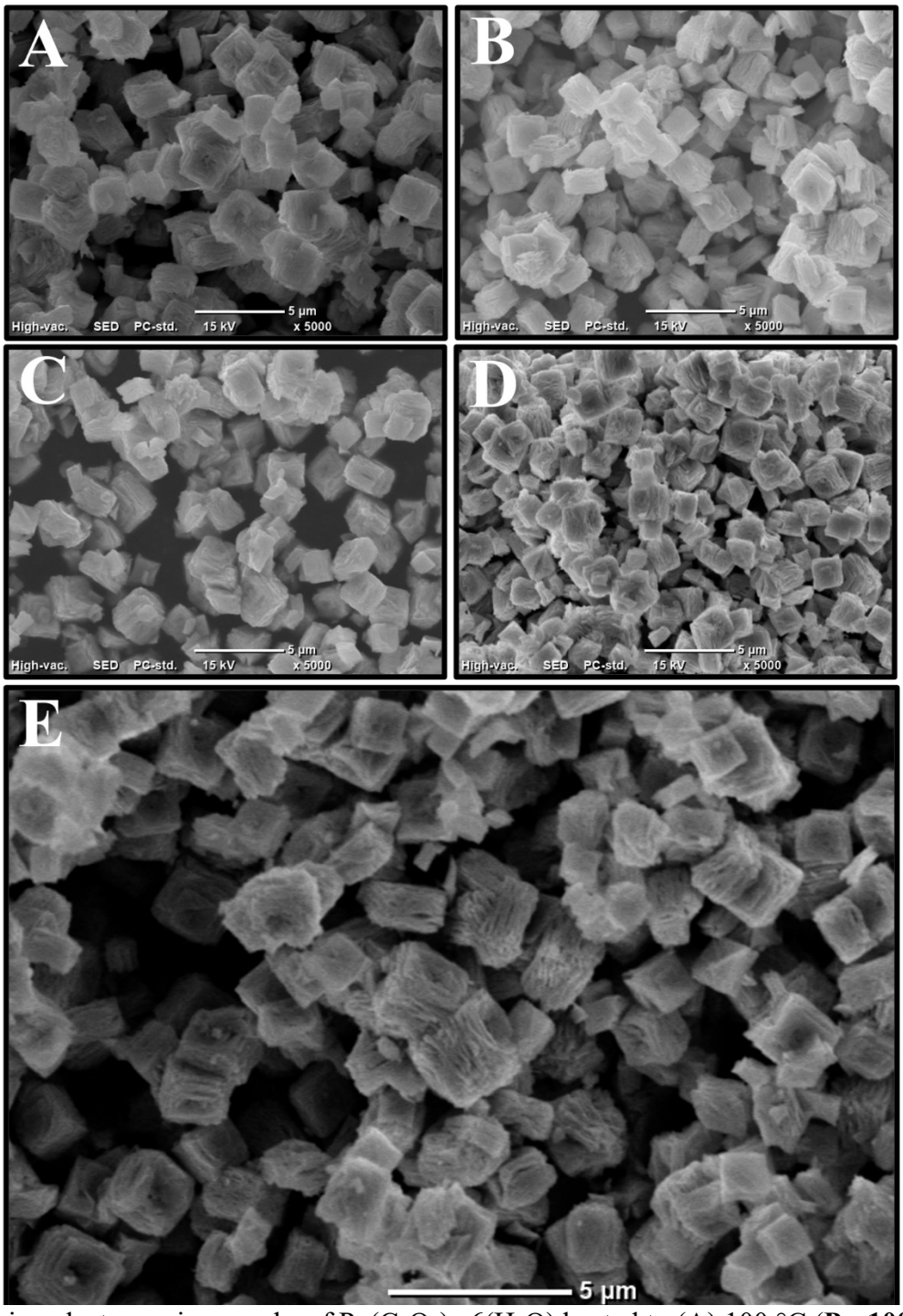

Fig. 5. Scanning electron micrographs of $Pu(C_2O_4)_2$•$6(H_2O)$ heated to (A) 100 °C (**Pu-100**), (B) 200 °C (**Pu-220**), (C) 250 °C (**Pu-250**), (D) 350 °C (**Pu-350**), and (E) 450 °C(**Pu-450**).

SUPPORTING INFORMATION

Raman and Infrared Spectra of Plutonium (IV) Oxalate and Its Thermal Degradation Products

Jonathan H. Christian[a,b], Bryan J. Foley[a], Elodia Ciprian[b], Don D. Dick[c], Meena Said[b,d], Jason Darvin[c], Amy Hixon[b*], Eliel Villa-Aleman[c*]

[a] Chemical Processing Section, Savannah River National Laboratory, Aiken, SC 29808 USA
[b] Department of Civil & Environmental Engineering & Earth Sciences, University of Notre Dame, Notre Dame, IN, 46556, USA
[c] Nuclear Nonproliferation Division, Savannah River National Laboratory, Aiken, SC 29808 USA
[d] Nuclear & Chemical Sciences Division, Lawrence Livermore National Laboratory, Livermore, CA, 94550 USA

*Corresponding Authors:
Eliel.Villa-Aleman@srnl.doe.gov
Amy.Hixon.2@nd.edu

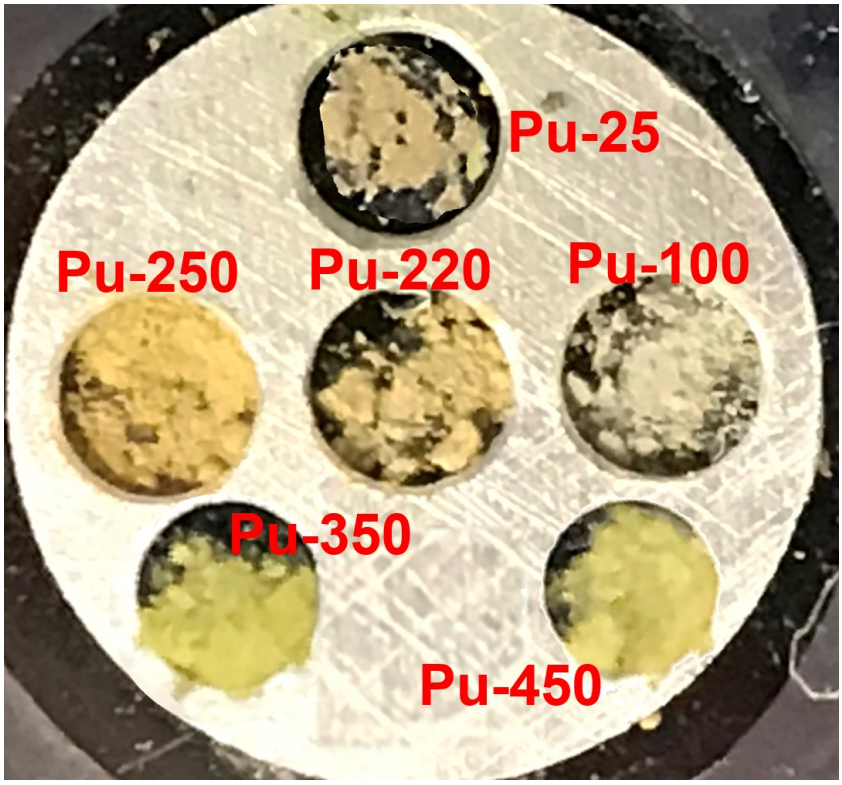

Fig. S1. Visual appearance of Pu(IV) oxalate produced at room temperature (**Pu-25**) and its degradation products up to 450 °C (**Pu-450**).

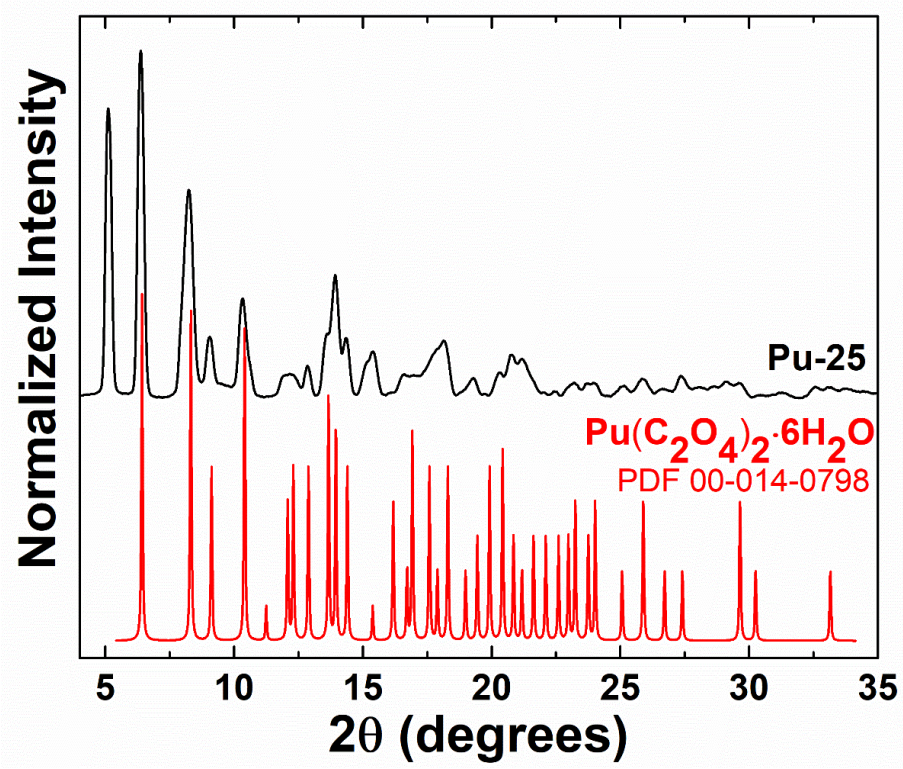

Fig. S2. The powder X-ray diffraction pattern of Pu(IV) oxalate produced at 25 °C is consistent with the powder diffraction file for $Pu(C_2O_4)_2 \cdot 6H_2O$ (PDF number 00-014-0798).[1] Broadening of the experimental pattern relative to the PDF pattern is due to instrument broadening, as pXRD measurements were acquired on a single-crystal X-ray diffractometer. Broadening may also exist due to differences in crystallite size, bulk crystallinity, and/or the presence of slightly amorphous material in the bulk sample, although no emperical evidence was gathered to support these claims.

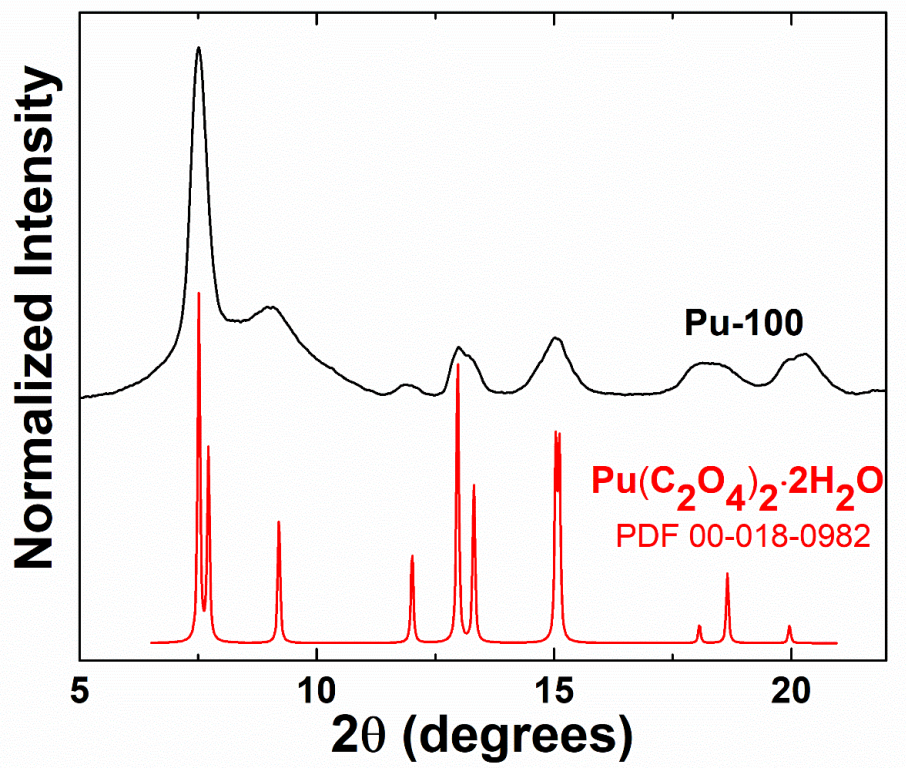

Fig. S3. The powder X-ray diffraction pattern of Pu(IV) oxalate heated to 100 °C is consistent with the powder diffraction file for $Pu(C_2O_4)_2 \cdot 2H_2O$ (PDF number 00-018-0982).[2] Broadening of the experimental pattern relative to the PDF pattern is due to instrument broadening, as pXRD measurements were acquired on a single-crystal X-ray diffractometer. Broadening may also exist due to differences in crystallite size, bulk crystallinity, and/or the presence of slightly amorphous material in the bulk sample, although no emperical evidence was gathered to support these claims.

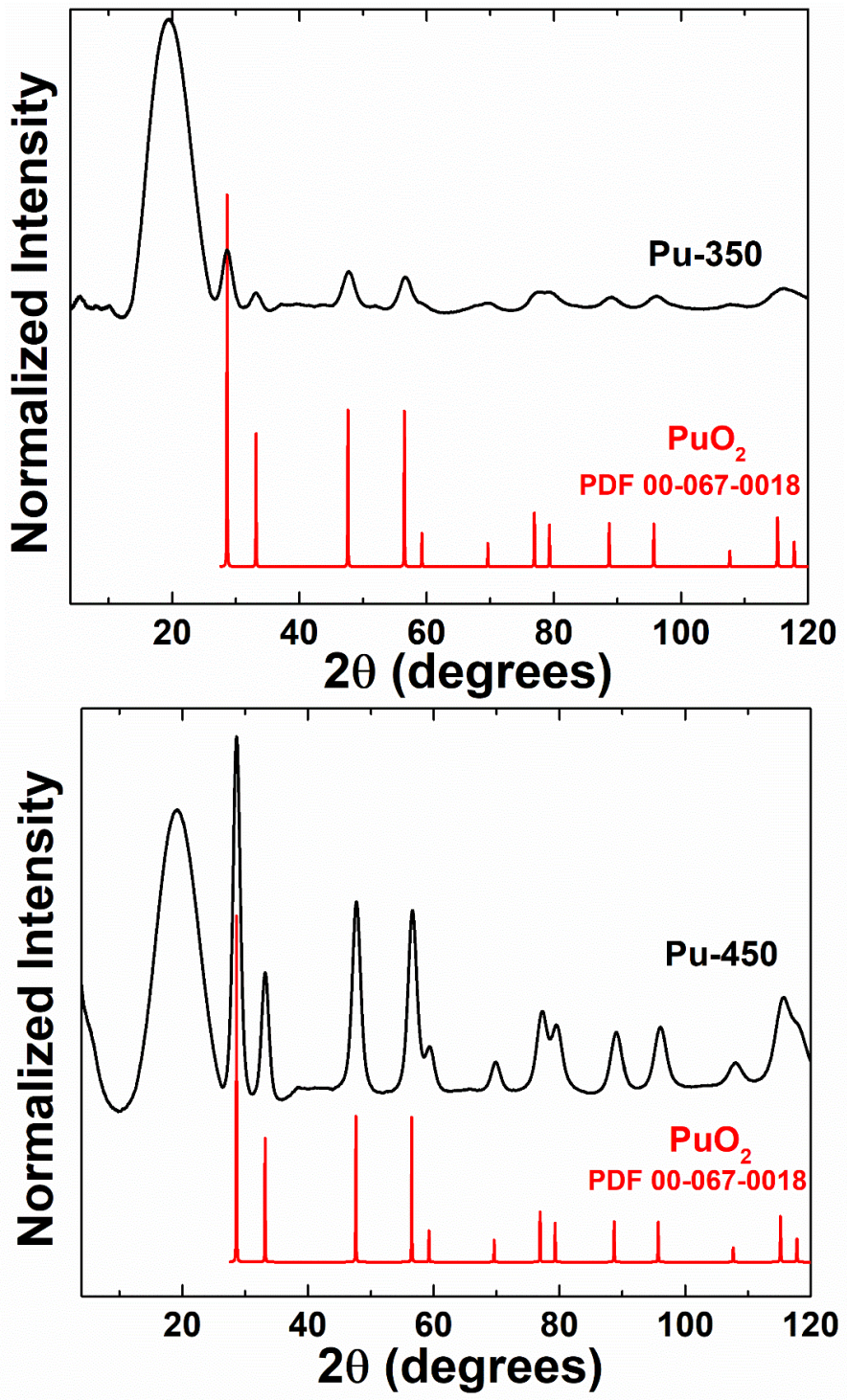

Fig. S4. The powder X-ray diffraction patterns of Pu(IV) oxalate heated to 350 °C (top) and 450 °C (bottom) are consistent with the powder diffraction file for PuO_2 (PDF number 00-067-0018).[3] Broadening of the experimental pattern relative to the PDF pattern is due to instrument broadening, as pXRD measurements were acquired on a single-crystal X-ray diffractometer. Broadening may also exist due to differences in crystallite size, bulk crystallinity, and/or the presence of slightly amorphous material in the bulk sample, although no emperical evidence was gathered to support these claims.